Ultrafast excited state dynamics in land plants Photosystem I core and whole supercomplex under oxidised electron donor conditions

Mattia Russo[1], Vasilis Petropoulos[1], Egle Molotokaite[2], Giulio Cerullo[1], Anna Paola Casazza[3], Margherita Maiuri[1*], Stefano Santabarbara[2*]

[1] IFN Consiglio Nazionale delle Ricerche, Dipartimento di Fisica, Politecnico di Milano, Piazza Leonardo da Vinci 32, 20133 Milano, Italy;

[2] Photosynthesis Research Unit, Centro Studi sulla Biologia Cellulare e Molecolare delle Piante, Consiglio Nazionale delle Ricerche, Via Celoria 26, 20133 Milano, Italy;

[3] Istituto di Biologia e Biotecnologia Agraria, Consiglio Nazionale delle Ricerche, Via Bassini 15a, 20133 Milano, Italy

*To whom correspondence should be addressed.

S.S. Centro Studi sulla Biologia Cellulare e Molecolare delle Piante, CNR, Via Celoria 26, 20133 Milano, Italy. Tel: + 39 02 503 14857; e-mail: stefano.santabarbara@cnr.it

M.M. Dipartimento di Fisica, Politecnico di Milano, P.zza Leonardo da Vinci 32, 20133 Milano, Italy. e-mail: margherita.maiuri@polimi.it

Abstract

The kinetics of excited state energy migration were investigated by femtosecond transient absorption in the isolated Photosystem I-Light Harvesting Complex I (PSI-LHCI) supercomplex and in the isolated PSI core complex of spinach under conditions in which the terminal electron donor P_{700} is chemically pre-oxidised. It is shown that under these conditions the relaxation of the excited state is characterised by lifetimes of about 0.4 ps, 4.5 ps, 15 ps, 35 ps and 65 ps in PSI-LHCI and 0.15 ps, 0.3 ps, 6 ps and 16 ps in the PSI core complex. Compartmental spectral-kinetic modelling indicates that the most likely mechanism to explain the absence of long-lived (ns) excited states is the photochemical population of a radical pair state, which cannot be further stabilised and decays non-radiatively to the ground state with time constants in the order of 6–8 ps.

Keywords: Photosystem I, Energy Transfer, Electron Transfer, Reaction centres, Photochemical Quenching

Abbreviation: PSI, Photosystem I; PSII, Photosystem II; LHCI, Light Harvesting Complex I; RC, Reaction Centre; ET, Electron Transfer, EET, Excited energy transfer, TA, Transient absorption; DADS, Decay associated differential absorption spectrum; SADS, Species associated difference absorption spectrum.

Introduction.

Photosystem I (PSI) is a key component of the photosynthetic electron transport chain, being involved both in linear electron transport, in conjunction with Photosystem II, as well as in cyclic electron transfer, where it is the sole photo-catalytic pigment-protein supercomplex involved (Croce and van Amerongen 2013; Caffarri et al. 2014). In land plants, PSI is located in the thylakoid membranes of the chloroplast, and it is built up by two functional and structural moieties: the core complex, where the charge separation (photochemical quenching) and the successive electron transfer (ET) reactions occur, and a so-called external antenna complement, collectively referred to as Light Harvesting Complex I (LHCI). The core complex, which also serves as light-harvesting antenna to the photocatalytic reaction centre (RC), comprises about 15 protein subunits (Croce and van Amerongen 2013; Caffarri et al. 2014). The vast majority of the chromophores, chlorophyll (Chl) *a* and β-carotene (β-car), bound to it are coordinated by the large heterodimer constituted by the PsaA and the PsaB subunits, that also binds all of the electron transfer (ET) cofactors with the exception of the terminal iron-sulphur clusters F_A and F_B which are coordinated by the PsaC subunit (Jordan et al. 2001; Amunts et al. 2010; Qin et al. 2015). The LHCI complement is instead composed by four Chl *a/b*-binding polypeptides, organised as pairs of protein heterodimers, Lhca1-4 and Lhca2-3 (Croce et al. 2002; Croce and van Amerongen 2013; Caffarri et al. 2014) that, according to structural studies, are harboured in a half-moon shape at the periphery of the super-complex (Ben-Shem et al. 2003; Dekker and Boekema 2005; Qin et al. 2015, Mazor et al. 2017).

PSI has some interesting photochemical properties. First, the quantum yield of photochemical conversion, *i.e.* the number of charge separated states formed per photon absorbed, approaches unity (Croce and van Amerongen 2013; Caffarri et al. 2014), making it one of the most efficient photochemical machineries known in Nature. Such high quantum efficiency is attained in PSI even though some light-harvesting antenna pigments absorb at lower energy than the RC chromophores (Gobets and van Grondelle 2001; Croce et al. 2002), implying a thermodynamically unfavourable uphill energy transfer to the photocatalytic site (Jennings et al. 2003a, 2013). In higher plants the low energy absorbing chromophores, that are often referred to as "red forms", are mainly located in the LHCI complement, where they are red-shifted by 10-15 nm with respect to the RC and 15-30 nm with respect to the so-called "bulk" Chl absorption (Croce et al. 1998, 2002; Jennings et al. 2003b; Croce and van Amerongen 2013). At least one red-shifted form, responsible for the characteristic low temperature emission centred at 730-735 nm, is associated with each of the Lhca1-4 and Lhca2-3 heterodimers (Wientjes and Croce 2011). Low energy sites in the antenna should in principle compete with the RC for the localization of the photoexcited energy, thereby decreasing the overall photochemical efficiency. Although some losses due to the presence of low energy forms in the

antenna are actually detected and manifest themselves as an increase in the average photochemical trapping time, which is the time required to populate a stabilised radical pair and can be determined from the average excited state lifetime (Jennings et al. 2003b), in the long wavelength emission tail (Croce et al. 2000; Engelman et al. 2006; Jennings et al. 2003a, 2013; Galka et al. 2012; Santabarbara et al. 2017; Molotokaite et al. 2017). The presence of red Chl forms results only in a very moderate decrease of the photon conversion efficiency, rarely exceeding a few (1-4) percents (Jennings et al. 2003a, 2013; Molotokaite et al. 2017). In line with these observations, also the increase in the external antenna dimension due to the formation of the PSI-LHCI-LHCII ternary supercomplex during the so-called State Transitions, a physiological process by which the antenna cross-sections of PSI and PSII are balanced when under PSI absorption is limiting , leads to only a minor decrease in the overall photochemical conversion yield (Galka et al. 2012; Wientjes et al. 2013; Le Quiniou et al. 2015; Akhtar et al. 2016; Santabarbara et al. 2017). This is true for the case of higher plants, when on average a single LHCII trimer leads to a ~20% increase in antenna size (Galka et al. 2012, Pan et al. 2018), as well as in the much larger supercomplex of the green alga *Chlamydomonas reinhardtii*, where the antenna dimension almost doubles with respect to the PSI-LHCI supercomplex (Drop et al. 2014, Nawrocki et al. 2016).

Another interesting photophysical property of PSI is that the excited state relaxation kinetics are very weakly dependent on the redox state of the RC cofactors (Byrdin et al. 2000; Giera et al. 2010). This is stark contrast with PSII, for which the fluorescence quantum yield increases by 4-5 fold when the ET reactions to the photosystem acceptor side are transiently blocked by intense light pulses or by the use of specific inhibitors (e.g. Butler 1978; Duysens 1978), a condition commonly referred to as “closed reaction centres”. This difference may be due to the fact that in PSI the terminal acceptors are further apart from the RC pigments than in PSII and therefore their transient reduction might not affect its primary photochemistry. On the other hand, the oxidised form of the photochemically generated electron donor P_{700}^{+} is rather long lived, from tens to hundred of microseconds *in vivo* (e.g. Haenel 1984; Hope 2000; Hervás et al. 2003) to tens/hundreds of milliseconds *in vitro* (e.g. Brettel 1997; Shinkarev et al. 2000), whereas its PSII counterpart, P_{680}^{+}, is reduced in tens of nanoseconds when the donor side of the photosystem is functional. Thus, at least *in vitro*, it is relatively simple to photo-accumulate P_{700}^{+} and a condition of “closed centres” can be induced in PSI, with the photochemically active pigments kept in their ionic state when successive light absorption events take place. Thus, analogously to what observed in PSII, the charge of P_{700}^{+} and its inability to further donate electrons is expected to impact on the charge separation reaction, thereby decreasing the efficiency of the photochemical quenching pathway. Yet, this expected event is generally not observed.

The almost insignificant change in the excited state relaxation kinetics under conditions in which P_{700} is in its ground state (open centres) or oxidised (P_{700}^{+}, closed centres) has been interpreted in terms of a direct quenching by P_{700}^{+}, since Chl cations are known to be good fluorescence quenchers (Butler 1978 and references therein). Yet, the almost perfect matching of the dynamics of photochemical quenching and non-photochemical quenching by P_{700}^{+} appears to be an odd coincidence. Most recently, a different hypothesis for the absence of fluorescence yield changes upon P_{700} oxidation has been put forward (Giera et al. 2010), stemming from the increasing evidence that the primary photochemically generated radical pair is stabilised by a successive, fast (less than 20 ps), secondary ET reaction. This "two-step" stabilisation model of the primary charge separation mechanism, originally proposed by Müller and coworkers (2003, 2010), implies a direct role as redox cofactors of the so-called "accessory" Chls, otherwise called Chl-eC2 according to the structural nomenclature of Jordan et al. (2001). Giera and coworkers (2010) proposed that a photochemical charge separation event might still occur when P_{700} is oxidised, but that the successive charge stabilisation step would be blocked, instead. In the absence of charge stabilisation, the primary radical pair would then be prone to a recombination reaction. Provided that the non-radiative recombination pathway to the ground state is comparable to the macroscopic overall charge stabilisation time constant, only small variations of fluorescence yield and excited state dynamics would then be observed.

In this study we use ultrafast optical spectroscopy to investigate the dynamics of excitation energy transfer (EET) in PSI of spinach, both in the isolated core complex and in the PSI-LHCI supercomplex, under conditions of closed reaction centres (P_{700}^{+}). This condition allows us to investigate EET dynamics in the absence of parallel deactivation channels associated with standard charge separation and charge stabilisation reactions. The experimental results confirm that, both in the core complex and the PSI-LHCI supercomplex, the kinetics are weakly affected by the redox state of P_{700}, as the main decay components remain substantially unaltered except for the disappearance of the long-lived signal belonging to the meta-stable $P_{700}^{+} - P_{700}$ spectrum. Moreover, the dynamics display only a limited dependence on the initial site of excitation, as inferred from tuning the pump wavelength in the 460-630 nm interval, with the sub-ps components showing the larger dependence. A process characterised by a lifetime of ~4-6 ps is observed in both samples. Due to its spectral features and as a result of spectral-kinetic modelling, this component could be assigned to the formation of a radical pair state from the RC excited state, even when P_{700} is pre-oxidised. These kinetics are similarly to what observed in PSI-LHCI under open centres conditions (e.g. Slavov et al. 2008; Molotokaite et al. 2017, Akhtar et al. 2016, 2018). However, the radical pair state does not

evolve toward a long-lived intermediate, but appears to decay non-radiatively with an effective time constant of about 6-8 ps (i.e. rate constants in the order of 130–160 ns^{-1}) thereby explaining the rapid excited state decay at closed centres.

Material and methods.

Biochemical purification. The PSI-LHCI supercomplex was isolated from spinach, as previously described (Molotokaite et al. 2017). The core complex was isolated starting from the PSI-LHCI supercomplex by solubilisation with a mixture of β-dodecyl maltoside (1% w/v) and Zwittergent-16 (0.5% w/v), for 20 min under gentle stirring in the dark at 4° C, and separated by sucrose gradient ultracentrifugation following the protocol described by Croce et al. (1998) for the *Zea mays* complex. The quality of the sample was estimated by absorption spectroscopy, as well as pigment and SDS-PAGE analysis. The absorption spectrum of the spinach core complex was indistinguishable from the previously reported one of the *Z. mays* preparation. Accordingly, Chl *b* was undetectable indicating, as confirmed by SDS-PAGE, that the purified core was almost fully depleted of the LHCI complement.

Ultrafast transient absorption experiments. The laser system employed for the transient absorption (TA) experiments is based on amplified Ti:Sapphire laser (Coherent Libra), with ~4 mJ output energy, 1 kHz repetition rate, central wavelength of 800 nm and pulse duration of 100 fs. A home-built optical parametric amplifier allows the generation of narrowband (~10 nm) pump pulses tuneable in the 480−650 nm wavelength range. A broadband white-light continuum probe pulse, covering the 450−740 nm wavelength range, was generated by focusing a fraction of the laser output into a 2-mm-thick sapphire plate. Pump and probe pulses were time delayed with respect to each other by a computer-controlled motorized translation stage. Pump and probe pulses, with relative polarization set to the magic angle, were focused into the 1-mm-thick sample cell to diameters of 340 and 150 μm, respectively. The transmitted probe beam was sent to a spectrometer equipped with a CCD sensor capable of recording spectra at the full 1 KHz laser repetition rate. The pump beam was modulated at 500 Hz by a mechanical chopper synchronized with the laser. Differential transmission ($\Delta T/T$) spectra as a function of probe wavelength, λ, and pump-probe delay, t, were obtained as $\Delta T/T(\lambda,t) = [T_{on}(\lambda,t) - T_{off}(\lambda)]/T_{off}(\lambda)$, where $T_{on}(\lambda,t)$ and $T_{off}(\lambda)$ are the transmitted probe spectra with and without the pump. For small values of $\Delta T/T$ one can approximate $-\Delta T/T \cong \Delta A$, where ΔA is the differential absorption.

Measurements conditions. For the measurements samples were resuspended in a medium containing 20 mM Tricine/NaOH (pH 7.8), 20 mM NaCl and 0.03% β-dodecyl maltoside to an optical density equivalent to ~5 O.D. cm^{-1} at 680 nm, i.e. close to maximal absorption in the Q_y band, in quartz cuvette having an optical path-length of 1 mm. "Closed centres" conditions were obtained by incubation with the oxidant potassium ferricyanide ($K_3Fe(CN)_6$, 2 mM), which is known to keep P_{700} in its cationic state. This was verified also from the absence of long-lived spectra attributable to the $P_{700}^{+} - P_{700}$ difference.

Data analysis. Global analysis of TA spectra was performed employing a laboratory written software, involving a convolution with a Gaussian shaped instrumental response function (FWHM 100 fs) and time-zero correction compensating for probe chirp effects by a fourth order polynomial function as previously described (Molotokaite et al. 2017).

Spectral-kinetic simulations based on the compartmental description of the photosystem, in which the rates of forward and reverse EET between compartments are constrained by detailed balance from the Boltzmann distribution, were performed as described by Molotokaite et al. (2017). The Boltzmann factors are then given by the number of Chl molecules present in each excited state compartment and by the mean excited state energy of the compartment that is determined by its spectral characteristics. This constrain cannot be applied, however, to compartments describing charge separation or ET processes. Further details are presented in the supplementary information, and when necessary, are discussed in the text (vide infra).

Results

PSI-LHCI supercomplex. Figure 1 shows the TA spectra recorded in the PSI-LHCI supercomplex isolated from spinach under chemically pre-oxidised P_{700} conditions, for representative pump-probe delays in the 100 fs to 1 ns range. A comparison is shown between excitations of PSI-LHCI at 480 nm (Figure 1a), a wavelength where carotenoids are preferentially excited, and at 620 nm (Figure 1b), where the higher vibronic bands of Chls are excited preferentially instead. Experiments were performed at fluence of 11 μJ/cm^2 (10 nJ/pulse) for both pump wavelengths, at which bimolecular annihilation effects were found to be negligible. Also shown in Figure 1 are the TA kinetics at selected probe wavelengths, together with their global fits. When the sample was excited at 480 nm (Figure 1c), a satisfactory description of the kinetics required 5 exponential components of 370 fs, 4.4 ps, 15.2 ps, 33 ps and 66 ps, as well as a very small-amplitude non-decaying component within the investigated time window. For excitation at 620 nm (Figure 1d), lifetimes of 370 fs, 4.5 ps, 15.3 ps, 33 ps and 66 ps together with a small-amplitude non-decaying component

were retrieved, in very good agreement with the previous values. The negligible contribution of non-linear processes to the kinetics is confirmed by the very close similarity of the lifetimes reported here and those retrieved by time-resolved fluorescence spectroscopy (e.g. Croce et al. 2000; Gobets and Van Grondelle 2001; Engelman et al. 2006; Slavov et al. 2008, Akhtar et al. 2016, Santabarbara et al. 2017) where excitation fluences are commonly more than two order of magnitude lower.

The decay-associated differential absorption spectra (DADS) resulting from the global analysis are shown in Figure 2a for excitation at 480 nm and Figure 2b for excitation at 620 nm. The results obtained using higher pump fluences (in the 20-50 μJ/cm^2 range) and in the absence of any redox mediator acting either as electron donor or acceptor were almost indistinguishable from those obtained in the presence of the oxidant $K_3Fe(CN)_6$.

The excited state dynamics in PSI-LHCI recorded when the terminal electron donor is in the cationic state, P_{700}^+, are remarkably similar to those observed in the same sample under open centres (neutral state of P_{700}), except for the absence, at closed centres, of a long-lived component associated to the P_{700}^+ *minus* P_{700} absorption difference (e.g. Molotokaite et al. 2017 and Supplementary Information Figure S1 where a direct comparison is presented). This observation confirms previous reports concerning PSI of other organisms, including green algae (Giera et al. 2010) and cyanobacteria (Byrdin et al. 2000; Shelaev et al. 2010), that P_{700} oxidation state does not affect largely the excites state relaxation dynamics.

Differences in the DADS retrieved from exciting in the blue region at 480 nm and in the red region at 620 nm are mainly observed for the fastest component, falling in the sub-picosecond time range, which appears to be dominated by EET processes from short-wavelength chromophore pools to the bulk Chls absorbing around 685-690 nm. Some differences are also notable in the ~4 ps DADSs which is also characterised by EET from the bulk to red-shifted Chls with absorption centred around 705-710 nm. Yet, whereas similar band-shapes on the long-wavelength absorption wing associated to a population rise are observed for both excitations, the amplitude of the associated bleaching is larger for excitation at 620 nm with respect to 480 nm. This component has been previously assigned to the population of the RC excited state as well as to primary charge separation (Müller et al. 2003, 2010; Molotokaite et al. 2017, Akhtar et al. 2018). However, charge separation dynamics are expected to be to some extent affected by the cationic state of P_{700} because of the charge localised in the vicinity of the cofactors potentially active in photochemical events. This will be discussed further below. The 15.5 ps component is the one with largest amplitude and describes the relaxation of the bulk Chls. The 33 ps DADS has a maximum bleaching corresponding to the absorption peak, but also shows a pronounced shoulder extending over the absorption tail, indicating a substantial contribution of long wavelength absorption forms to this kinetic phase. The 66 ps component describes almost exclusively

the relaxation of red-shifted absorption forms centred around 710-715 nm, with very limited contributions of the bulk Chl forms.

PSI core complex. Figure 3 shows the TA spectra recorded in the core complex of PSI, also isolated from spinach, for excitations at 490 nm (Figure 3a) and 630 nm (Figure 3b) under conditions of chemically pre-oxidised P_{700}. TA spectra are presented for similar pump-probe delays as for the whole PSI-LHCI supercomplex (Figure 1). Figure 3c/d also reports the TA kinetics at representative probe wavelengths, together with the fits resulting from the global analysis, whereas the retrieved DADS are shown in Figure 4a (pump at 490 nm, 8 nJ/pulse) and Figure 4b (pump at 630 nm, 3 nJ/pulse). Also in the core complex, very similar results are obtained when exciting with higher pump fluences (15-30 nJ/pulse) and in the absence of redox mediators (Supplementary Information Figure S2 and Figure S3). Four exponential components characterised by lifetimes of 140 fs, 330 fs, 5.7 ps and 16 ps, when pumping at 490 nm, and 130 fs, 315 fs, 5.6 ps and 16.5 ps, when pumping at 630 nm, were required to globally describe the kinetics. In both cases also a small-amplitude long-lived component had to be considered. These lifetime values are very close to those obtained for the PSI-LHCI supercomplex, but two sub-picosecond components were retrieved in the core, whereas the longer 33 ps and 66 ps components were not detected instead. The latter observation is in agreement with fluorescence lifetime measurements on similar complexes from land plants (Engelman et al. 2006; Slavov et al. 2008; Wientjes et al. 2011; Jennings et al. 2013, Santabarbara et al. 2017). The two fastest components, which also show some pump-wavelength dependence, appear to be associated to EET between different antenna pigment pools, with the fastest lifetime (~150 fs) reflecting mainly transfer to short-wavelength absorbing pigments among the bulk Chls either from the vibrational states of Chls and/or from inter-molecular relaxation from higher singlet energy levels of the so-called Soret band, as well as transfer from carotenoids, when exciting at 490 nm. Especially upon excitation in the vibronic Chl band (630 nm), stimulated emission (SE) resulting from the relaxation of both vibronic and higher excited state (e.g. Q_x transition) is also likely to contribute to this DADS. The differences observed in the band-shape of the ~150 fs component, whose life time is, however, close to our temporal resolution, might be due to different relative contributions of EET and SE processes. The ~350 fs component appears to reflect mainly transfer from short to longer wavelength Chls, covering the bulk of the antenna absorption.

This resembles what observed in PSI-LHCI under open centre conditions where only the DADS associated to the fastest and the ~4 ps components had a band-shape that depended significantly on the excitation wavelength in the 480-630 nm window (Molotokaite et al. 2017). The results of the global fit analysis for the experiments performed in the PSI core complex using pump

pulses tuned in the 460-570 nm window are presented in the Supplementary Material (Figure S4). Similarly to what observed in the PSI-LHCI supercomplex, the sub-picosecond components display only a moderate dependence on the pump wavelength. Moreover, the DADS associated to the ~5 ps component shows remarkable similarities to the one retrieved for the whole PSI-LHCI supercomplex (Molotokaite et al. 2017), involving population transfer from short to long wavelength Chl forms having an apparent maximum at approximately 700 nm and a rather broad bandwidth. A component having very similar characteristics was also retrieved from the analysis of two-dimensional electronic spectroscopy (2DES) in the visible of both the core and the PSI-LHCI supercomplex isolated from pea (Akhtar et al. 2018). It should, however, be noticed that, upon excitation at 490 nm (Figure 4a, and similarly but less markedly, for pumping at 460 nm, Figure S4), the ~5 ps DADS appears to show also an additional contribution, centred at about 680 nm, which might be due to residual, relatively slow, EET processes probably from carotenoids due to the relatively large absorption of these chromophores with respect to Chls at these pump wavelengths. In all conditions, the 16 ps component is the largest and dominant one, describing what appears to be a homogenous ground state repopulation of the bulk Chls.

Discussion

In this study we have compared the excited state relaxation kinetics in the PSI-LHCI supercomplex and in the PSI core complex under conditions in which the terminal electron donor P_{700} is initially pre-oxidised. P_{700} was kept in its cationic state by chemical oxidation, and the kinetics recorded at relatively low pump fluences, thereby almost eliminating possible contribution from non-linear processes such as singlet-singlet exciton annihilation. Under these conditions, one would expect that the presence of a closed RC at the moment of excitation would prevent the formation of a long-lived radical pair, irrespectively of the exact sequence of primary and secondary charge separation events. Thus, the excited state should reside mainly in the antenna and its decay should be dominated by the intrinsic relaxation processes, that for Chls bound to proteins correspond to time constants in the 2-4 ns range.

Contrary to these general expectations, these experiments confirm that, when both PSI-LHCI and the PSI core complex are excited in the presence of P_{700}^{+}, the relaxation of the excited state remains rapid. The relaxation kinetics, moreover, display only a relatively moderate dependence on the excitation wavelength, as shown here for the core complex (Figure S4) and previously for the PSI-LHCI supercomplex (Molotokaite et al. 2017) at least when pumping in the 450–630 nm window, which all represents higher energies with respect to the one of the reaction centre. Due to large spectral crowding in PSI, the tested wavelength shall produce only limited differences in the initial site of

excitation, i.e. core antenna with respect to the external antenna in the supercomplex, or the bulk antenna with respect to the RC for both samples investigated. On the other hand, more significant dependences are expected upon excitation in the long wavelength absorption edge, which have been indeed documented at least for the case of cyanobacterial core complexes (Gobets et al. 2001, 2003, Semenov et al. 2012, Cherepanov et al. 2017a,b), whereas only partial information is available for higher plant complexes and limited, to our knowledge, to the recent 2DES study of Akhatar et al. (2018).

The most significant difference in between measurements performed under open and closed RC conditions is then the absence of signals arising from the formation of the meta-stable P_{700}^{+} species in the latter, which confirms the "closed state" of the RC. To interpret the rapid excited state decay at closed centres, it is necessary to postulate the presence of a process capable of quenching the excited state even in the absence of long-lived charge separated states.

In order to further address the physical mechanism responsible for this fast decay, an extension of the spectral-kinetic model simulations recently presented by Molotokaite et al. (2017) was here implemented. We opted for a spectral-kinetic simulation approach which is aimed at a semi-quantitative description of the results, rather than global-target fitting. Although the latter could, in principle, provide more accurate information as it aims for an exact description of the experimental dataset, kinetic modelling approach allows to impose physical-based constraints on the "tuneable" simulations parameters which are more difficult, although not impossible, to implement when aiming for an exact data description. The principal constraint employed here is that the ratio of the forward and reverse communication rates between compartments shall be governed by the Boltzmann distribution. The Boltzmann factors are determined by the number of Chls present in each compartment and their mean excited state energies which, in turn, depend on their associated spectra. The number of pigments in each compartment can be reasonably derived from independent structural and/or biochemical evidences, whereas the mean excited state energies are determined by the spectral characteristics of each compartment. The mean excited state energy is better estimated from the compartment fluorescence emission, which was explicitly considered in the original model developed for open centres conditions (Molotokaite et al. 2017). Within this approach, only the forward rates and the spectra are adjustable parameters, whereas the back reaction rates become fully constrained thereby significantly decreasing the number of free running simulation parameters. This is, however, true only for communications between excited state compartments, whereas for ET reactions, forward and reverse rates are tuneable. Since this approach is aimed only at a semi-quantitative description of the results, the values of the rate constants are, whenever possible, rounded, whereas target analysis can provide more accurate estimation in principle. On the other hand, since the model employed here

does not describe any specific set of data, it might have the benefit of describing the system in a more general fashion albeit at the expenses of precision. Moreover, strategies for simultaneous, and computationally efficient, target-fitting of data resulting from different experimental approaches have not been developed yet. Although this might be an interesting approach for future investigations, the starting model employed here was shown already to be capable of satisfactorily describing, with semi-quantitative accuracy, both TA and time-resolved fluorescence kinetics in the spinach PSI-LHCI supercomplex under open centre conditions. It is worth mentioning that, although this model contained the novel aspect of simultaneously describing fluorescence and TA kinetics, it also incorporated several elements stemming from previous investigations. For instance, the presence of heterogeneous excited state transfer dynamics from the low energy forms (here indicated as Red_1^* and Red_2^*), is in agreement with previous fluorescence lifetime studies of PSI-LHCI supercomplexes from land plants (Croce et al. 2000; Engelman et al. 2006; Jennings et al. 2003a; Wientjes et al. 2011; Santabarbara et al. 2017). This is also consistent with the presence of at least one long-wavelength Chl form in each of the two heterodimers composing the LHCI complement (Wientjes and Croce 2011). Moreover, the occurrence of a sequential two-step charge separation/stabilisation mechanism on the picosecond time scale, together with the presence of a significant degree of reversibility of the primary charge separated state, also derived from previous analysis of ultrafast TA data (Müller et al. 2003, 2010).

The rational here utilised to implement the "closed centres" (P_{700}^+) model, is that of including as minimal as possible alterations to the starting one, as shown in Figure 5a. For instance, all the species associated spectra (SADS, Figure 6a) and the EET rates amongst the antenna compartments were those already reported, since these are not expected to be affected by the presence of P_{700}^+ in the RC. Moreover, it was assumed that a charge separation event could still occur, leading to the formation of a radical pair state ($RP_{1,C}$), but that, differently from the open centres conditions, this would not be followed by further ET steps. The parameters which were instead considered to differ from the "open centres" conditions were: i) the rate constants and the SADS (Figure 6a) associated to the population of the $RP_{1,C}$ radical pair state, since this species could either involve different chromophores with respect to RP_1 , the primary radical pair formed under open centres conditions, or its spectrum could be affected by the nearby charge on P_{700} ; ii) the SADS (Figure 6a) of the reaction centre excited state (RC^*) and the rate of the bulk antenna repopulation from RC^* , since both these factors could be affected by the presence of P_{700}^+ , as well.

It was found that, as shown in Figure 6c, with rather contained alterations with respect to the "open centres" model, the kinetics and DADS experimentally detected under closed centres could be

satisfactorily simulated. A slower value of the charge separation rate constant (550 ns^{-1} with respect to 645 ns^{-1}) and a small increase in the recombination rate to RC^* (45 ns^{-1} with respect to 40 ns^{-1}) had to be considered under closed centre conditions (Table 1). Also a modest blue shift of the mean energy of the RC^* compartment was adopted, consistently with the absence of the P_{700} absorption. We noticed however that the mean energy of RC^* remains red-shifted, at 710 nm (1.75 eV) with respect to the bulk of the antenna, which peak at about 699 nm (1.77 eV). The red shift with respect to the main ground state absorption bleaching is due to the presence of moderately red-shifted states in the LHCI antenna that, when taken into account, causes a redistribution of the excited-state population towards lower energies. We notice however that the amplitude of RC^* SADS is significantly larger than both the one of $Bulk^*$ and RP_{1c}, whereas, in principle, similar extent of bleaching are expected if each spectrum were to be dominated by ground state bleaching (GSB) contributions. These discrepancies could result from the limited accuracy inherent in the semi-quantitative approach employed, but they can also stem from the overlap of different signal contributions (e.g. excited state absorption (ESA) and stimulated emission (SE)), as well as for the differential nature of SADS. For instance, in the RC^* spectrum, the GSB and ESA contributions, which have opposite sign, appear better spectrally separated, thereby leading to a lower cancellation effect in the overlap region.

Crucially, in order to describe the experimental results, it was necessary to include a non-radiative de-excitation constant of 150 ns^{-1} from the radical pair $RP_{1,C}$, which is not present under "open conditions". At the same time, it was not possible to simulate the experimental data by excluding $RP_{1,C}$ and by considering a non-radiative de-excitation constant directly from RC^*, as this led to a failure in reproducing the 4-ps experimental DADS.

The general robustness of the description is confirmed by the fact that the model derived for the PSI-LHCI supercomplex can be straightforwardly extended to the PSI core complex (Figure 5b). In the core, it was not necessary to consider the presence of red forms that, in land plants, are a dominant characteristic feature of the external antenna. The absence of the external antenna is also accounted for by the decreased number of pigments in the $Bulk^*$ compartment (86 sites instead of 160 in the whole photosystem, corresponding to the chlorophyll binding stoichiometry) and by a blue shift of the mean energy of this compartment, 690 nm (1.79 eV), as expected since the residual long-wavelength contributions are also mostly associated with the LHCI complement. The SADS spectrum associated with both RC^* and $RP_{1,C}$ was instead basically the same as in the PSI-LHCI supercomplex (Figure 6b). It was found that to obtain satisfactory simulation of the experimental results acquired in the core complex, it was necessary to consider a constant of 350 ns^{-1} for the population of $RP_{1,C}$, together with a non-radiative relaxation characterised by a rate constant of 125 ns^{-1}. The simulations

of the DADS extracted from the global fits of the experimental traces are in figure 6d. It is worth stressing that also in the core complex it was necessary to include the population of the $RP_{1,C}$ radical pair in order to simulate the 5-ps DADS.

The rapid relaxation of the excited state under conditions in which P_{700} is pre-oxidised is therefore associated to the presence of a ~120-150 ns^{-1} rate constant from the $RP_{1,C}$ radical pair. Our data do not allow to assign with precision the nature of this radical pair state, although the associated SADS spectrum indicates the involvement of relatively red-shifted Chls (Figure 6a,b). The more likely involved chromophores are the Chls indicated as eC_2 and eC_3, the latter corresponding to A_0, in the crystallographic model (Jordan et al. 2001). The eC_2 Chls have been proposed to act as primary electron donor even under open conditions (Müller et al. 2003, 2010). Yet, it is not unreasonable to envisage that different charge separation paths can occur depending on the redox state of the other cofactors composing the RC, as the operative potentials of both donors and acceptors will be affected by nearby charge on P_{700}^{+}. For instance, charge separation leading to the initial population of the [$P_{700}^{+}eC_2^{-}$], followed by the $P_{700}^{+}eC_3^{-}$, *i.e.* implying electron transfer between eC_2^{-} and eC_3 rather than a hole transfer between eC_2^{+} and P_{700}, as a secondary step, could not be entirely ruled out under open centres conditions. This pathway would, however, be certainly blocked upon pre-oxidation of P_{700}.

It appears that $RP_{1,C}$ cannot be further stabilised and it either repopulates RC^{*}, according to the reversible radical pair model originally proposed by Holzwarth and coworkers (Müller et al. 2003, 2010), or it is otherwise dissipated through the process characterised by the ~130 ns^{-1} rate constant. The overall EET dynamics at closed centres are then determined largely by the competition between these two processes, but in the absence of the dissipative process the overall would be dominated by natural de-excitation from the excited state compartments (i.e. in ~ 2 ns, since a rate of 0.5 ns^{-1} was considered in the kinetic simulations). The non-radiative dissipative pathway retrieved from ultrafast TA data modelling is consistent with a charge recombination reaction that directly repopulates the ground state of the cofactors composing $RP_{1,C}$, in agreement with what proposed by Gibasiewicz and coworkers (Giera et al. 2010) on the basis of time-resolved fluorescence measurements performed on PSI of green algae.

Acknowledgments.

SS and APC acknowledge support for this research from Fondazione Cariplo (CYAO project), Grant Number 2016-0667, and thank Dr. A. Petrova for the assistance in biochemical sample preparation. GC acknowledges support from the PRIN 2017 project 201795SBA3 – HARVEST. VP,

GC and MM acknowledge financial support from the Marie Sklodowska-Curie project 812992-MUSIQ.

Conflict of Interest: The authors declare that they have no conflict of interest.

Figure Legends.

Figure 1. Transient absorption (TA) spectra of the PSI-LHCI supercomplex recorded at selected pump-probe delays, as indicated in the legend, upon excitation at 480 nm (a) or 620 nm (b). TA kinetics in the PSI-LHCI supercomplex upon excitation at 480 nm (c, closed symbols) and 620 nm (d, open symbols) recorded at selected probe wavelengths. Symbols: experimental data-points (binned in 2.5 nm boxcar windows before being subjected to global fitting analysis); lines: global fits results. The samples were pre-incubated with potassium ferricyanide (2 mM) to maintain the electron donor P_{700} in oxidised conditions, which will hereafter referred to as closed centres. The full-width at half maximum (FWHM) of the excitation pulses was approximately 10 nm, and the pulse fluence was 11 μJ/cm^2 (10 nJ/pulse) for both excitations. All traces are normalised to the maximal ground state bleaching at the specific pump wavelength.

Figure 2. Decay Associated Differential Absorption Spectra (DADS) resulting from the global fits of the kinetics recorded in the PSI-LHCI supercomplex under closed centre conditions, upon excitation at 480 nm (a, closed symbols) and 620 nm (b, open symbols). The DADS are normalised to the maximal ground state bleaching of the ~15 ps component.

Figure 3. TA spectra of PSI core complex recorded at selected pump-probe delays (indicated in the legend) upon excitation at 490 nm (a) and 630 nm (b), both with a FWHM of about 10 nm, and fluences of 10 μJ/cm^2 (8 nJ/pulse) and 4.5 μJ/cm^2, (4 nJ/pulse) respectively. TA kinetics recorded in the core of PSI under closed centres conditions at selected probe wavelengths (indicated in the legend) when pumped at 490 nm (c, closed symbols) and 630 nm (d, open symbols). Symbols: experimental data-points (binned in 2.5 nm boxcar windows before being subjected to global fitting analysis); lines: global fit analysis results. The samples were pre-incubated with potassium ferricyanide (2 mM) to maintain closed centres conditions. All traces are normalised to the maximal ground state bleaching at the specific pump wavelength.

Figure 4. Decay Associated Differential Absorption Spectra (DADS) resulting from the global fits of the kinetics recorded in the PSI core complex under closed centres conditions, upon excitation at 490 nm (a, closed symbols) and 630 nm (b, open symbols). The DADS are normalised to the maximal ground state bleaching of the ~16 ps component.

Figure 5. Kinetic models utilised to simulate the transient absorption kinetics in PSI-LHCI supercomplex (a) and PSI core complex (b) of land plants, under close centres conditions. Both models were adapted from the one previously presented by Molotokaite et al. (2017) developed for PSI-LHCI at open centres. The dashed-dotted grey boxes and lines indicate the compartments which have not been considered due to closed centres conditions (a), or that are not relevant in the core but present in the whole supercomplex (b). The simulated population evolutions of each compartment considered for the modelling of PSI-LHCI and PSI core complex are presented in panels (c) and (s), respectively. The rate constants are reported in Table 1 and further details are discussed in the main text and in section 4 of the supplementary information.

Figure 6. Species-associated differential absorption spectra (SADS) employed for modelling of the DADS in PSI-LHCI (a) and PSI core complex (b) and simulated DADS for PSI-LHCI supercomplex (c) and PSI core complex (d).

References

Akhtar P, Lingvay M, Kiss T, Deák R, Bóta A, Ughy B, Garab G, Lambrev PH (2016) Excitation energy transfer between Light-harvesting complex II and Photosystem I in reconstituted membranes. Biochim. Biophys. Acta 1857:462–472

Akhtar P, Zhang C, Liu Z, Tan HS, Lambrev PH (2018) Excitation transfer and trapping kinetics in plant photosystem I probed by two-dimensional electronic spectroscopy. Photosynth. Res. 135:239–250

Amunts A, Toporik H, Borovikova A, Nelson N (2010) Structure determination and improved model of plant photosystem I. J. Biol. Chem. 285:3478 – 3486

Ben-Shem A, Frolow F, Nelson N (2003) Crystal structure of plant photosystem I. Nature 426:630–635

Brettel K (1997) Electron transfer and arrangement of the redox cofactors in Photosystem I. Biochim. Biophys. Acta 1318: 322–373

Butler QL (1978) Energy distribution in the photochemical apparatus of photosynthesis, Ann Rev Plant Physiol 29: 345–378

Byrdin M, Rimke I, Schlodder E, Stehlik D, Roelofs TA (2000) Decay kinetics and quantum yields of fluorescence in Photosystem I from *Synechococcus elongatus* with P_{700} in the reduced and oxidized state: are the kinetics of excited state decay trap-limited or transfer-limited? Biophys. J. 79:992–1007

Caffarri, S, Tibiletti, T, Jennings, RC, Santabarbara, S (2014) A Comparison between Plant Photosystem I and Photosystem II architecture and functioning. Curr. Protein Pept. Sci. 15:296–331

Cherepanov DA, Shelaev IV, Gostev FE, D Mamedov MD, Petrova AA, Aybush AV, Shuvalov VA, Semenov AY, Nadtochenko VA (2017a) Excitation of photosystem I by 760 nm femtosecond laser pulses: transient absorption spectra and intermediates, J. Phys. B. 50: 174001 – 174009

Cherepanov DA, Shelaev IV, Gostev FE, Mamedov MD, Petrova AA, Aybush AV, Shuvalov VA, Semenov AY, Nadtochenko VA. (2017b) Mechanism of adiabatic primary electron transfer in photosystem I: Femtosecond spectroscopy upon excitation of reaction center in the far-red edge of the Qy band, Biochim. Biophys. Acta 1858:895–905

Croce R, Zucchelli G, Garlaschi FM, Jennings RC (1998) A thermal broadening study of the antenna chlorophylls in PSI-200, LHCI, and PSI core. Biochemistry 37:17355–17360

Croce R, Dorra D, Holzwarth AR, Jennings RC (2000) Fluorescence decay and spectral evolution in intact photosystem I of higher plants, Biochemistry 39:6341–6348

Croce R, Morosinotto T, Castelletti S, Breton J, Bassi R (2002) The Lhca antenna complexes of higher plants Photosystem I. Biochim. Biophys. Acta 1556:29–40

Croce R, van Amerongen H (2013) Light-harvesting in photosystem I. Photosynth. Res. 116:153–166

Dekker JP, Boekema EJ (2005) Supramolecular organization of thylakoid membrane proteins in green plants Biochim. Biophys. Acta 1706:12–39

Drop B, Yadav K N S, Boekema EJ, Croce R. (2014) Consequences of state transitions on the structural and functional organization of photosystem I in the green alga *Chlamydomonas reinhardtii.* Plant J. 78:181–191

Duysens LNM (1978) Transfer and trapping of excitation energy in photosystem II, Ciba Found Symp. 323–340.

Engelmann E., Zucchelli G, Casazza AP, Brogioli D, Garlaschi FM, Jennings RC (2006) Influence of the photosystem I-light harvesting complex I antenna domains on fluorescence decay. Biochemistry 45:6947–6955

Galka P, Santabarbara S, Khuong TT, Degand H, Morsomme P, Jennings RC, Boekema EJ, Caffarri S (2012) Functional analyses of the plant photosystem I-light-harvesting complex II supercomplex reveal that light-harvesting complex II loosely bound to photosystem II is a very efficient antenna for photosystem I in state II. Plant Cell 24:2963–2978

Giera W, Ramesh VM, Webber AN, van Stokkum IHM, van Grondelle R, Gibasiewicz K (2010) Effect of the P_{700} pre-oxidation and point mutations near A_0 on the reversibility of the primary charge separation in Photosystem I from *Chlamydomonas reinhardtii*. Biochim Biophys Acta 1797:106–112

Gobets B, van Grondelle R. (2001) Energy transfer and trapping in Photosystem I, Biochim. Biophys. Acta 1057:80–99

Gobets B, van Stokkum IH, Rögner M, Kruip J, Schlodder E, Karapetyan NV, Dekker JP, van Grondelle R. (2001) Time-resolved fluorescence emission measurements of photosystem I particles of various cyanobacteria: a unified compartmental model, Biophys. J. 81:407–424

Gobets B, van Stokkum IH, van Mourik F, Dekker JP, van Grondelle R. (2003) Excitation wavelength dependence of the fluorescence kinetics in Photosystem I particles from *Synechocystis* PCC 6803 and *Synechococcus elongatus*, Biophys. J. 85:3883–3898

Haehnel W. (1984) Plastocyanin. Annu. Rev. Plant Physiol. 35:659–693

Hervás M, Navarro JA, De La Rosa MA (2003) Electron transfer between membrane complexes and soluble proteins in photosynthesis. Acc. Chem. Res. 36: 790–805

Hope AB (2000) Electron transfer amongst cytochrome *f*, plastocyanin and Photosystem I: kinetics and mechanism. Biochim. Biophys. Acta 1456:5–26

Jennings RC, Zucchelli G, Croce R, Garlaschi FM (2003a) The photochemical trapping rate from red spectral states in PSI-LHCI is determined by thermal activation of energy transfer to bulk chlorophylls. Biochim. Biophys. Acta 1557:91–98

Jennings RC, Garlaschi FM, Engelmann R, Zucchelli G (2003b) The room temperature emission band shape of the lowest energy chlorophyll spectral form of LHCI. FEBS Lett. 547:107–110

Jennings RC, Zucchelli G, Santabarbara S (2013) Photochemical trapping heterogeneity as a function of wavelength, in plant photosystem I (PSI-LHCI). Biochim. Biophys. Acta 1827:779–785

Jordan P, Fromme P, Witt HT, Klukas O, Saenger W, Krauss N (2001) Three-dimensional structure of cyanobacterial photosystem I at 2.5 Å resolution. Nature 411:909–917

Le Quiniou C, van Oort B, Drop B, van Stokkum IHM, Croce R (2015) The high efficiency of Photosystem I in the green alga *Chlamydomonas reinhardtii* is maintained after the antenna size is substantially increased by the association of Light-Harvesting Complexes II. J. Biol. Chem. 290:30587–30595

Mazor Y, Borovikova A, Caspy I, Nelson N (2017) Structure of the plant photosystem I supercomplex at 2.6Å resolution. Nat Plants 3:17014

Molotokaite E, Remelli W, Casazza AP, Zucchelli G, Polli D, Cerullo G, Santabarbara S (2017) Trapping dynamics in Photosystem I-Light Harvesting Complex I of higher plants is governed by the competition between excited state diffusion from low energy states and photochemical charge separation. J. Phys. Chem. B. 121:9816–9830

Müller MG, Niklas J, Lubitz W, Holzwarth AR (2003) Ultrafast transient absorption studies on Photosystem I reaction centers from *Chlamydomonas reinhardtii.* 1. A new interpretation of the energy trapping and early electron transfer steps in Photosystem I. Biophys. J. 85:3899–3922

Müller MG, Slavov C, Luthra R, Redding KE, Holzwarth AR (2010) Independent initiation of primary electron transfer in the two branches of the Photosystem I reaction center. Proc. Natl. Acad. Sci. U.S.A 107:4123–4128

Nawrocki WJ, Santabarbara S, Mosebach L, Wollman FA, Rappaport F (2016) State transitions redistribute rather than dissipate energy between the two photosystems in Chlamydomonas. Nat Plants. 2:16031

Pan X, Ma J, Su X, Cao P, Chang W, Liu Z, Zhang X, Li M (2018) Structure of the maize photosystem I supercomplex with light-harvesting complexes I and II. Science 360:1109–1113

Qin X, Suga M, Kuang T, Shen JR (2015) Photosynthesis. structural basis for energy transfer pathways in the plant PSI-LHCI supercomplex. Science 348:989–995

Santabarbara S, Tibiletti T, Remelli W, Caffarri S (2017) Kinetics and heterogeneity of energy transfer from light harvesting complex II to Photosystem I in the supercomplex isolated from arabidopsis. Phys. Chem. Chem. Phys. 19:9210–9222

Semenov AY, Shelaev IV, Gostev FE, Mamedov MD, Shuvalov VA, Sarkisov OM, Nadtochenko VA. (2012) Primary steps of electron and energy transfer in photosystem I: effect of excitation pulse wavelength. Biochemistry (Mosc). 77:1011–1020

Shelaev IV, Gostev FE, Mamedov MD, Sarkisov OM, Nadtochenko VA, Shuvalov VA, Semenov AY (2010) Femtosecond primary charge separation in *Synechocystis sp.* PCC 6803 Photosystem I. Biochim. Biophys. Acta 1797:1410–1420

Shinkarev VP, Vassiliev IR, Golbeck JH (2000) A kinetic assessment of the sequence of electron transfer from F_X to F_A and further to F_B in Photosystem I: the value of the equilibrium constant between F_X and F_A. Biophys J. 78:363–372

Slavov C, Ballottari M, Morosinotto T, Bassi, R, Holzwarth AR (2008) Trap-limited charge separation kinetics in higher plant Photosystem I complexes. Biophys J. 94:3601–3612

Wientjes E, Croce R (2011) The light-harvesting complexes of higher-plant Photosystem I: Lhca1/4 and Lhca2/3 form two red-emitting heterodimers. Biochem. J. 433:477–485

Wientjes E, van Stokkum IH, van Amerongen H, Croce R (2011) The role of the individual Lhcas in photosystem I excitation energy trapping. Biophys. J. 101:
745–754

Wientjes E, van Amerongen H, Croce R (2013) LHCII is an antenna of both photosystems after long-term acclimation. Biochim. Biophys. Acta 1827:420–426

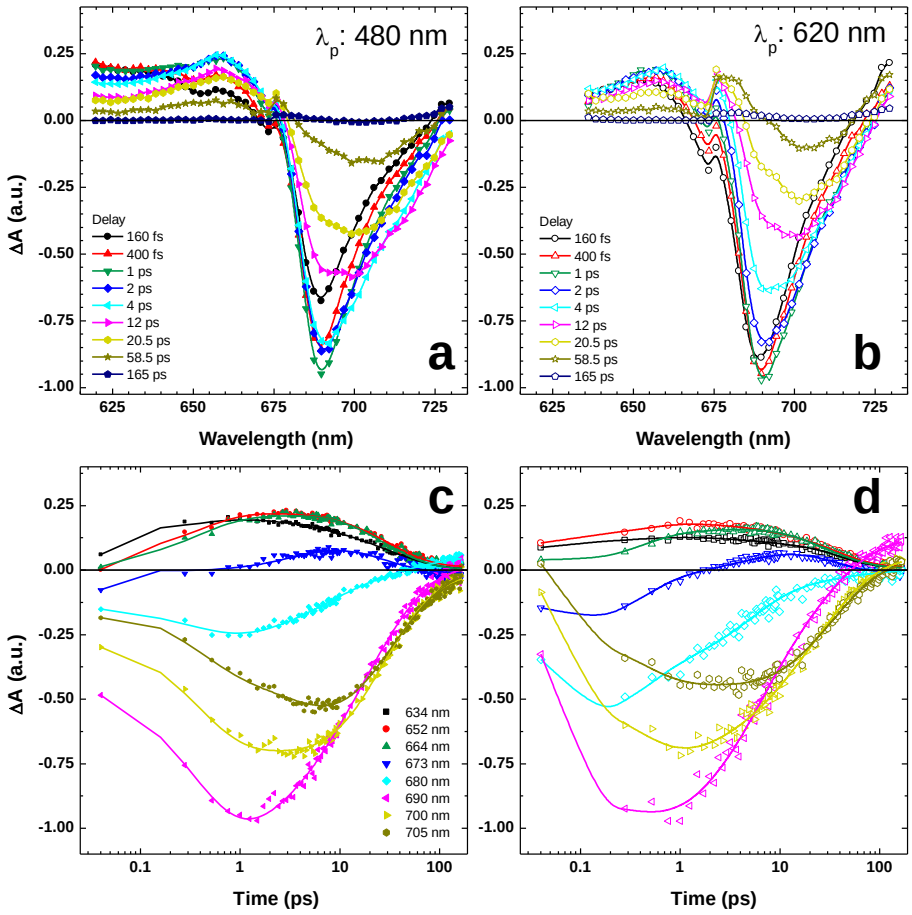

Figure 1. Transient absorption (TA) spectra of the PSI-LHCI supercomplex recorded at selected pump-probe delays, as indicated in the legend, upon excitation at 480 nm (a) or 620 nm (b). TA kinetics in the PSI-LHCI supercomplex upon excitation at 480 nm (c, closed symbols) and 620 nm (d, open symbols) recorded at selected probe wavelengths. Symbols: experimental data-points (binned in 2.5 nm boxcar windows before being subjected to global fitting analysis); lines: global fits results. The samples were pre-incubated with potassium ferricyanide (2 mM) to maintain the electron donor P_{700} in oxidised conditions, which will hereafter referred to as closed centres. The full-width at half maximum (FWHM) of the excitation pulses was approximately 10 nm, and the pulse fluence was 11 μJ/cm^2 (10 nJ/pulse) for both excitations. All traces are normalised to the maximal ground state bleaching at the specific pump wavelength.

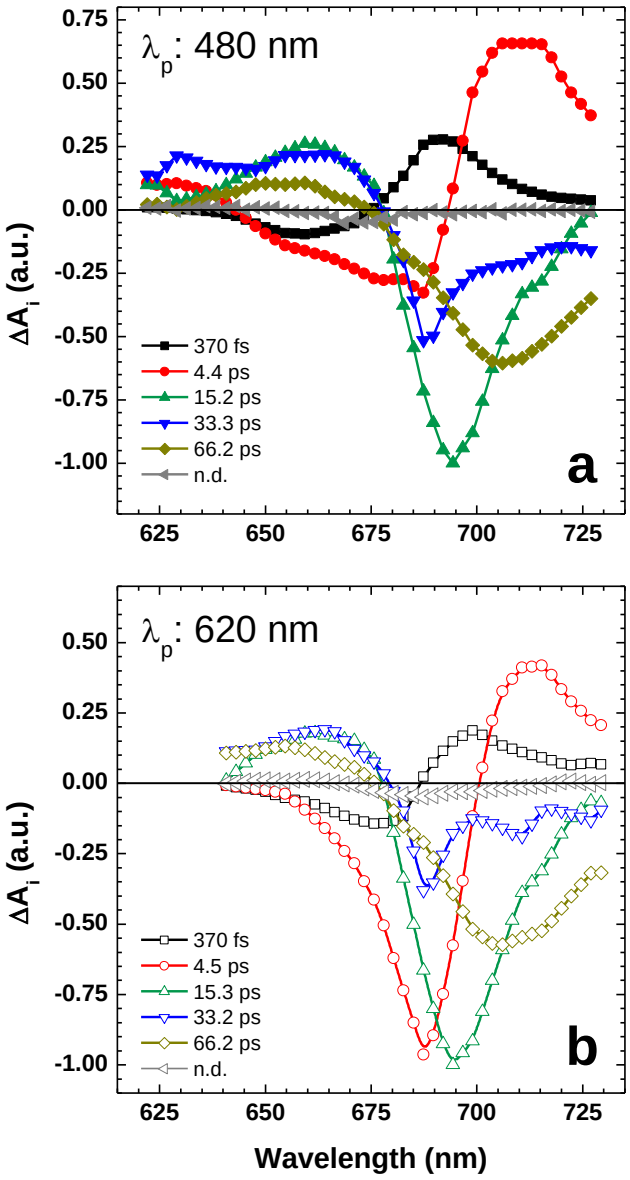

Figure 2. Decay Associated Differential Absorption Spectra (DADS) resulting from the global fits of the kinetics recorded in the PSI-LHCI supercomplex under closed centre conditions, upon excitation at 480 nm (a, closed symbols) and 620 nm (b, open symbols). The DADS are normalised to the maximal ground state bleaching of the ~15 ps component.

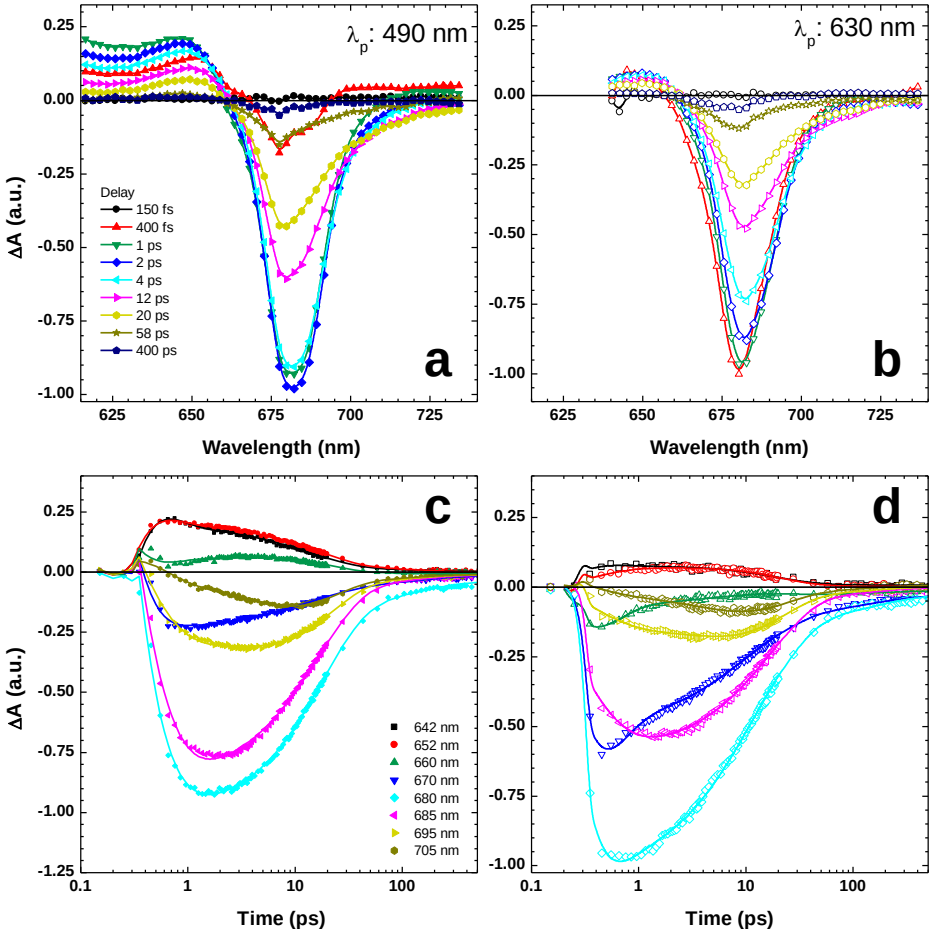

Figure 3. TA spectra of PSI core complex recorded at selected pump-probe delays (indicated in the legend) upon excitation at 490 nm (a) and 630 nm (b), both with a FWHM of about 10 nm, and fluences of 10 μJ/cm^2 (8 nJ/pulse) and 4.5 μJ/cm^2, (4 nJ/pulse) respectively. TA kinetics recorded in the core of PSI under closed centres conditions at selected probe wavelengths (indicated in the legend) when pumped at 490 nm (c, closed symbols) and 630 nm (d, open symbols). Symbols: experimental data-points (binned in 2.5 nm boxcar windows before being subjected to global fitting analysis); lines: global fit analysis results. The samples were pre-incubated with potassium ferricyanide (2 mM) to maintain closed centres conditions. All traces are normalised to the maximal ground state bleaching at the specific pump wavelength.

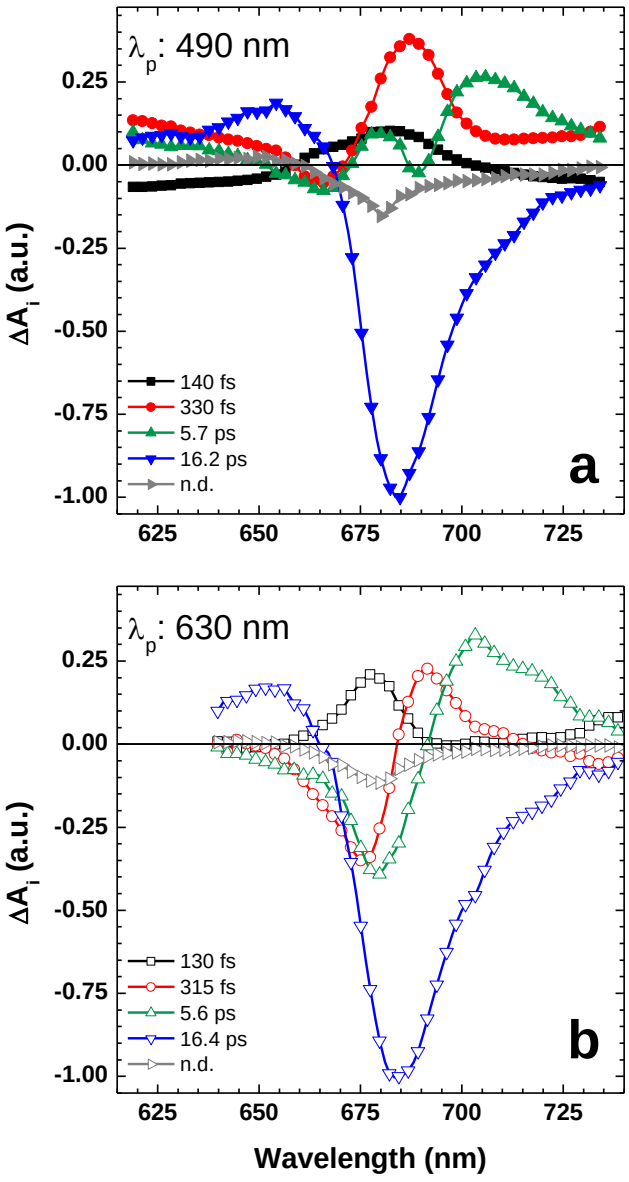

Figure 4. Decay Associated Differential Absorption Spectra (DADS) resulting from the global fits of the kinetics recorded in the PSI core complex under closed centres conditions, upon excitation at 490 nm (a, closed symbols) and 630 nm (b, open symbols). The DADS are normalised to the maximal ground state bleaching of the ~16 ps component.

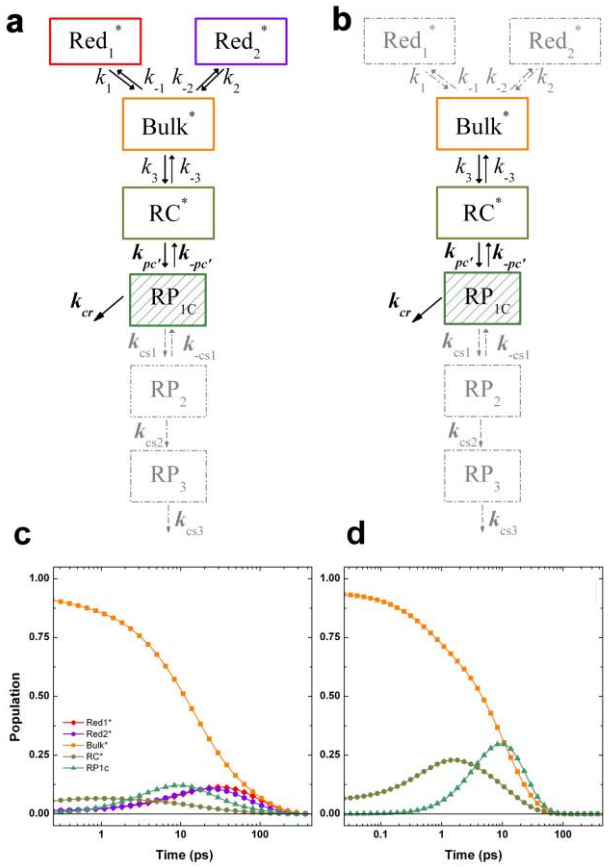

Figure 5. Kinetic models utilised to simulate the transient absorption kinetics in PSI-LHCI supercomplex (a) and PSI core complex (b) of land plants, under close centres conditions. Both models were adapted from the one previously presented by Molotokaite et al. (2017) developed for PSI-LHCI at open centres. The dashed-dotted grey boxes and lines indicate the compartments which have not been considered due to closed centres conditions (a), or that are not relevant in the core but present in the whole supercomplex (b). The simulated population evolutions of each compartment considered for the modelling of PSI-LHCI and PSI core complex are presented in panels (c) and (s), respectively. The rate constants are reported in Table 1 and further details are discussed in the main text and in section 4 of the supplementary information.

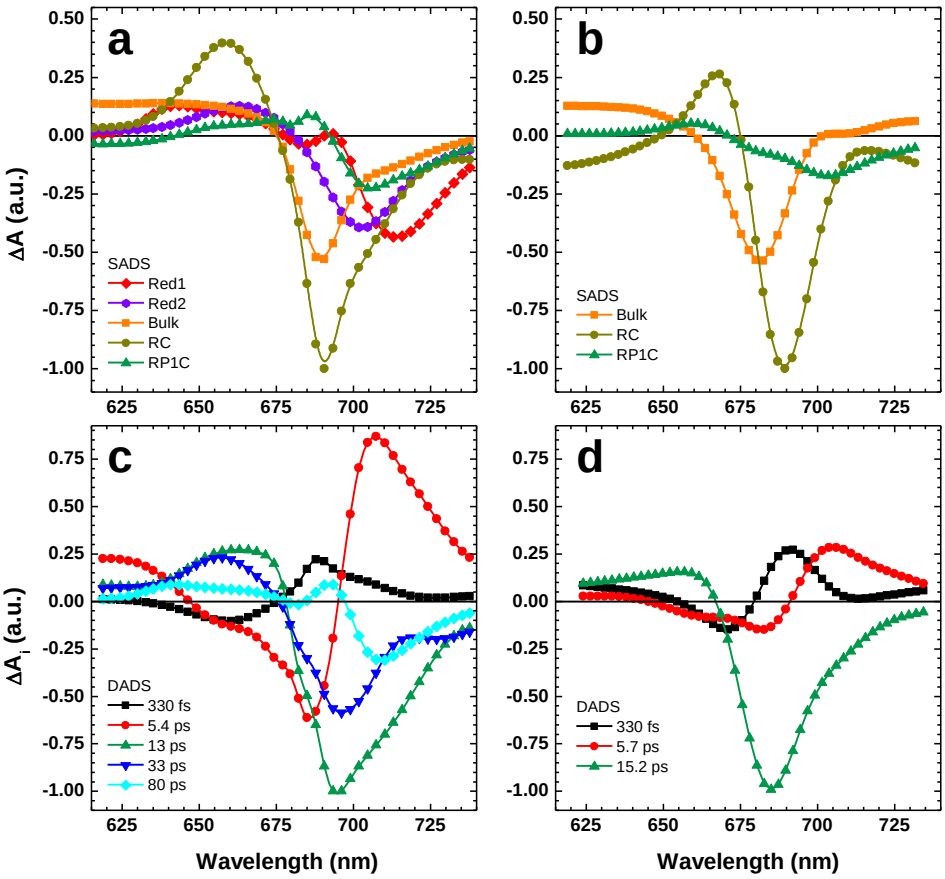

Figure 6. Species-associated differential absorption spectra (SADS) employed for modelling of the DADS in PSI-LHCI (a) and PSI core complex (b) and simulated DADS for PSI-LHCI supercomplex (c) and PSI core complex (d).

Table 1. Rate constants employed in kinetic simulations

PSI-LHCI		
	k_i (ns^{-1})	k_{-i} (ns^{-1})
$Red_1^* \rightleftarrows Bulk^*$	26	12
$Red_2^* \rightleftarrows Bulk^*$	41	14
$Bulk^* \rightleftarrows RC^*$	265	2450[§]
$RC^* \rightleftarrows RP_{1,c}$	550	45

PSI Core		
	k_i (ns^{-1})	k_{-i} (ns^{-1})
$Bulk^* \rightleftarrows RC^*$	500	1110
$RC^* \rightleftarrows RP_{1,c}$	350	30

Sets of rate constants used in the simulations of LHCI-PSI and the PSI core samples. The mean energies of the excited state compartments (and site degeneracy, n_i, *i.e.* number of Chl pigments) were as follows: $\bar{E}_{Red1}$=1.68 eV (n_i=2), $\bar{E}_{Red2}$=1.69 eV (n_i=2), $\bar{E}_{bulk}$=1.77 eV (n_i=160) and $\bar{E}_{RC*}$ =1.75 eV (n_i=5). In the PSI core the mean energies of excited state compartments and site degeneracy were as follows: $\bar{E}_{bulk}$=1.79 eV (n_i=86) and $\bar{E}_{RC*}$=1.75 eV (n_i=5). The values of k_{cr} for PSI-LHCI and PSI core are 150 ns^{-1} and 125 ns^{-1} respectively.

[§]The upper limit for the rate constants, approaching singlet-singlet hopping time, was considered to be 2500, hence close to this value essentially determined by the large number of Chls in $Bulk^*$ with respect to RC^*.